Materials Research Proceedings **32** (2023) 338-354 https://doi.org/10.21741/9781644902615-39

Improved stochastic dissimilar diffusion bonding model with experimental validation

Bryan Ferguson[1,a], Neha Kulkarni[1,b], D.G. Sanders[1,c], Eric Bol[1,d *], and M. Ramulu[1,e *]

[1]Department of Mechanical Engineering, Box 352600, University of Washington, Seattle, WA 98195, USA

[a] bjferg@uw.edu, [b] nehamech2004@gmail.com, [c] southernstargold@comcast.net, [d] boled84@gmail.com, [e] ramulum@uw.edu

Keywords: Diffusion Bonding, Voids, Superplastic Forming, Statistical Modeling

Abstract. Diffusion bonding is a solid-state welding operation that has seen wide spread use in the aerospace industry, especially in combination with superplastic forming. It combines two relatively flat, clean surfaces at high temperature to create a near flawless weld over a large surface area. Modelling of diffusion bonding has been challenging due in part because of the larger variations in voids formed from the mating surfaces. This paper attempts to compensate for that inadequacy by implementing a stochastic diffusion bonding model based with theoretical voids formed from interacting surfaces. The model uses a statistical version of Pilling's model in combination with surface roughness based initial conditions that estimates the possibilities of voids formed. The results of the model are compared with experimental results for three different alloys at a variety of process conditions along with presenting an investigation of the mechanics of the model for future improvements.

Introduction

Diffusion bonding is a solid-state welding operation that welds two mating surfaces together at nearly the structural properties of the parent materials. The process is commonly used in the aerospace industry in combination with superplastic forming which allows one to selectively weld and form multiple sheets to create complex stiffened structures for considerable weight and maintenance savings [1]. It also has the advantage of being able to weld different metals together and/or dissimilar alloys to produce new material systems. The bonding process requires excellent surface preparation and occurs at temperatures around 50%-70% of the material melting temperature. The primary defects in diffusion bonded parts are voids that are formed at the interface between the surfaces due to slight misfit of the surface topography. These voids are closed via plastic deformation, power law creep, and several high temperature diffusive processes [2].

Plastic deformation, creep, and diffusion are all dependent on the temperature, the applied pressure, the bonding time, and the material properties of the alloys used. Additionally, the size of the voids determines how much material will need to transfer to close them. This results in a large dependence on the surface geometry which has been the subject of several studies [3–5]. The purpose of this research is to both improve upon the existing modeling, as well as to demonstrate a more accurate way of accounting for the initial void geometry by providing more complex information about the surfaces and the way voids are formed. This model specifically deals with titanium alloys that are important to aerospace due to their extremely high strength to weight ratio and corrosion resistance. Titanium has good fracture toughness and forms a variety of alloys with varied properties. Both similar and dissimilar alloy combinations were modeled since it is often necessary to bond dissimilar titanium alloys to take advantage of differences in formability, strength, and corrosion resistance depending upon varied performance requirements.

Materials Research Proceedings **32** (2023) 338-354 https://doi.org/10.21741/9781644902615-39

Prior attempts at providing an accurate model that can predict diffusion bonding processing conditions date back to the 1970s. These models can be separated into groups that deal with void closure with pressure sintering models, and groups that deal with void closure solely using diffusion and superplastic collapse. The pressure sintering models include surface diffusion around the void and model creep with power law creep, while the alternative uses superplastic instead of creep and do not include any surface diffusion. The other significant difference between models is how they model surfaces and void geometry. Hamilton published the initial attempt to solve the problem in 1973 and modeled the voids as infinitely long pyramidal shapes and the closure process as solely superplastic collapse [6].

Derby and Wallach provided the next major step that used Hamilton's initial geometry and approach and then applied pressure sintering equations to incorporate diffusion. The closure of voids was based on the mechanisms of initial plastic collapse of the contacting points, surface and volume diffusion into the void from surface sources, surface and volume diffusion from the bonding interface, and power law creep collapse [7–9]. More models by Takahashi and Guo used lenticular voids with a combination of diffusion and power law creep collapse [10,11]. Hill et al. provided improvements to the Derby model using the same mechanisms, but deriving the equations for elliptical geometry [2].

Pilling et al. created several models starting in 1984 specifically for Ti-6Al-4V (Ti-64). These models were derived from research on void formation during superplasticity and models the bonding behavior as closure by a combination of superplastic collapse and stress-based diffusion. The models neglected the bonding mechanisms of surface diffusion included in the Derby and Hill models, and the initial model geometry was cylinders on the diffusion bonding plane as voids [12]. The second model developed by Pilling used the same mechanisms, but with cylinders oriented perpendicular to the diffusion bonding plane [13]. This model is the basis for the current stochastic diffusion bonding model. Salehi and Pilling looked into the effects of using the same equations, but with different void geometry, and rewrote Pilling's second model equations for oblate spheroids instead of vertical cylinders [14]. Orhan [15] and Ma [16] created more complex versions of Ti-64 models that coupled the two theories together. Li created the first version of the probabilistic model based on the Pilling 1988 model [17]. The stochastic formulation of Pilling's model was expanded for dissimilar alloys by Kulkarni [18].

The most important characteristic of these models is their accuracy and ability to predict the bonding processing parameters. While most of the models make some comparison with experimental data, the models present their results in different ways and are for different materials and processing conditions making a direct comparison between models challenging. The models dealing with titanium bonding, the subject of this study, compare with experimental results without micrographic correlation. They use results from structural shear tests and compare the shear strength in binary form (bonded or not bonded for a processing condition for above or below 95% shear strength) to the calculated bonding time. However, there is no set standard for structural testing the shear strength in diffusion bonding. Several papers that have discussed different methods have pointed to the discrepancies in the testing and lack of ability to distinguish between higher bonding percentages [19]. It is therefore debatable that the results were accurate. More importantly, these models are not modeling the shear strength or structural characteristics of the void but instead just modeling void closure. A summary of all the different models that are compared with Pilling's experimental data are presented in Figure 1.

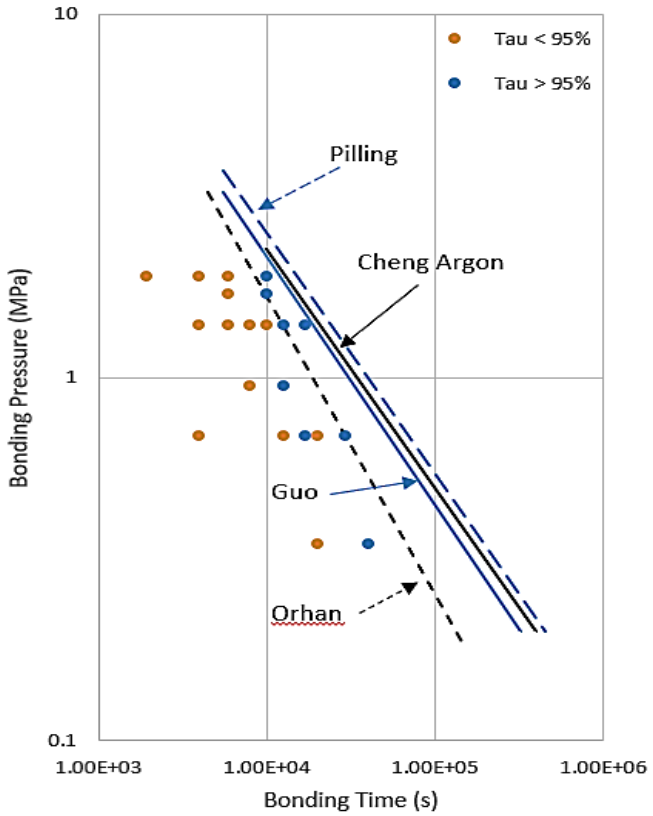

Figure 1: Bonding models compared with experimental results.

Experimental Methods

The model presented in this work uses a stochastic formulation, similar to Kulkarni et al., for dissimilar diffusion bonding with the inclusion of different initial conditions. Surface roughness profiles are interacted to determine the initial geometries of the voids followed by developing a statistical distribution based on them. This idea of overlapping the surfaces to determine the potential voids and then running statistics on them was pioneered by Kulkarni. The model in this paper provides a much more robust way of determining the potential voids.

The distribution of voids are applied to the equations derived by Pilling in a stochastic manner in the form of a Monte Carlo simulation. The surface roughness dataset is comprised of six different surface roughness profiles for each of the three materials for a total of 18 profiles. Three titanium alloy materials were involved which were TI-54M, Ti-64 standard grain, and Ti-6242S. Each material was prepared as it would be for diffusion bonding, and then surface profiles were measured using a Mahr XR20 MIT GD25 contact surface profilometer in random locations with three in the longitudinal direction and three in the transverse direction. Figure 2 displays the raw data for each profile which was aligned horizontally by subtracting a single linear fit of the data from the profile, not the series of linear fits commonly used in surface roughness measurements.

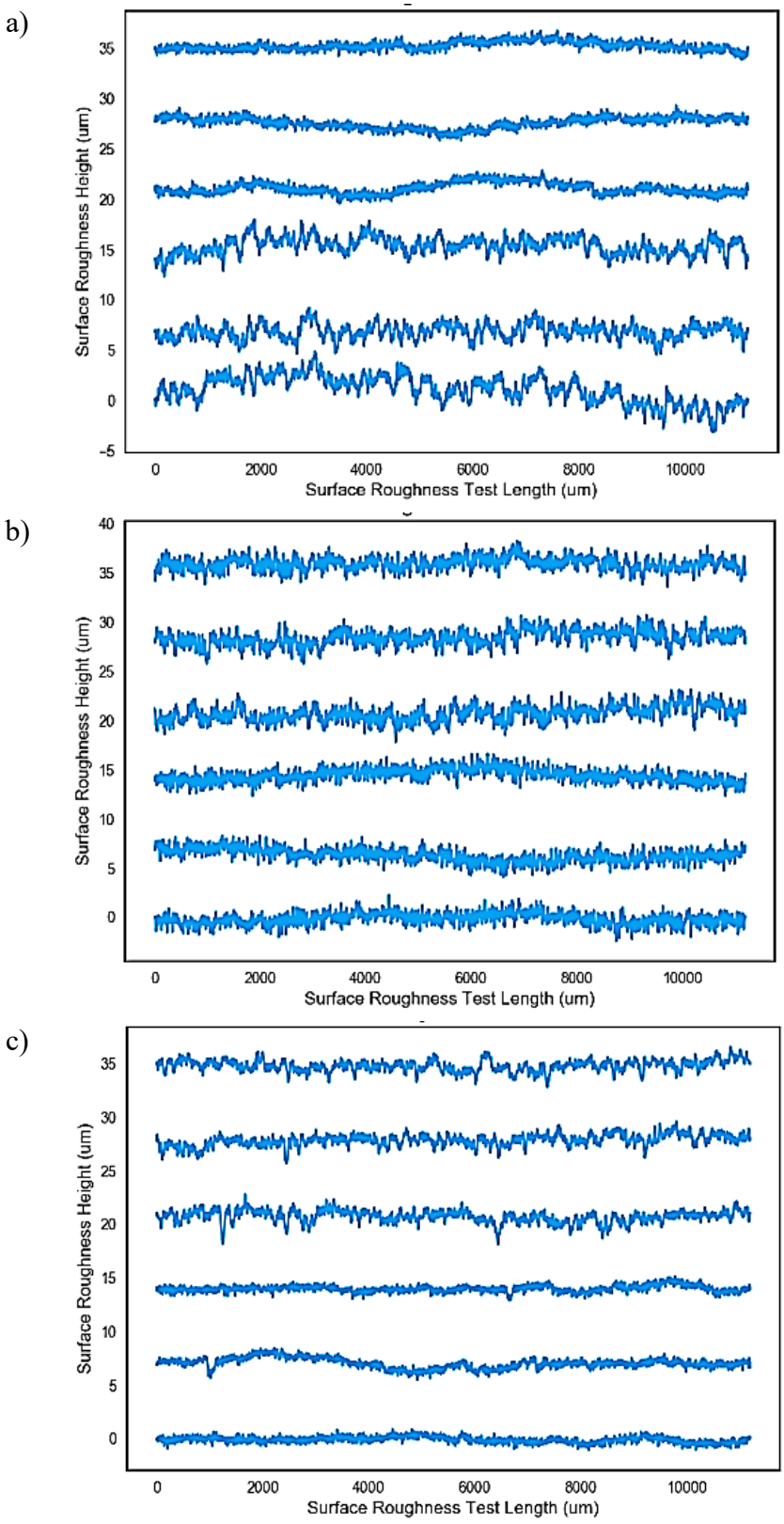

Figure 2: Surface roughness profiles from a) Ti54m, b) Ti6242S, and c) Ti64.

The initial conditions for the diffusion bonding model are based on the interaction of the two surfaces. The peaks of the surfaces contact and observe very high stresses causing them to go

through an initial plastic deformation and flatten out. This occurs until the flow stress reaches the superplastic region. In the current model, the reduction in void height is assumed to be a simple overlap of the surface roughness profiles and that the initial plasticity of the peaks results in negligible closure of the voids. This initial collapse provides very little closure to begin with but serves to define the initial void geometry which has a large effect on the overall bonding time.

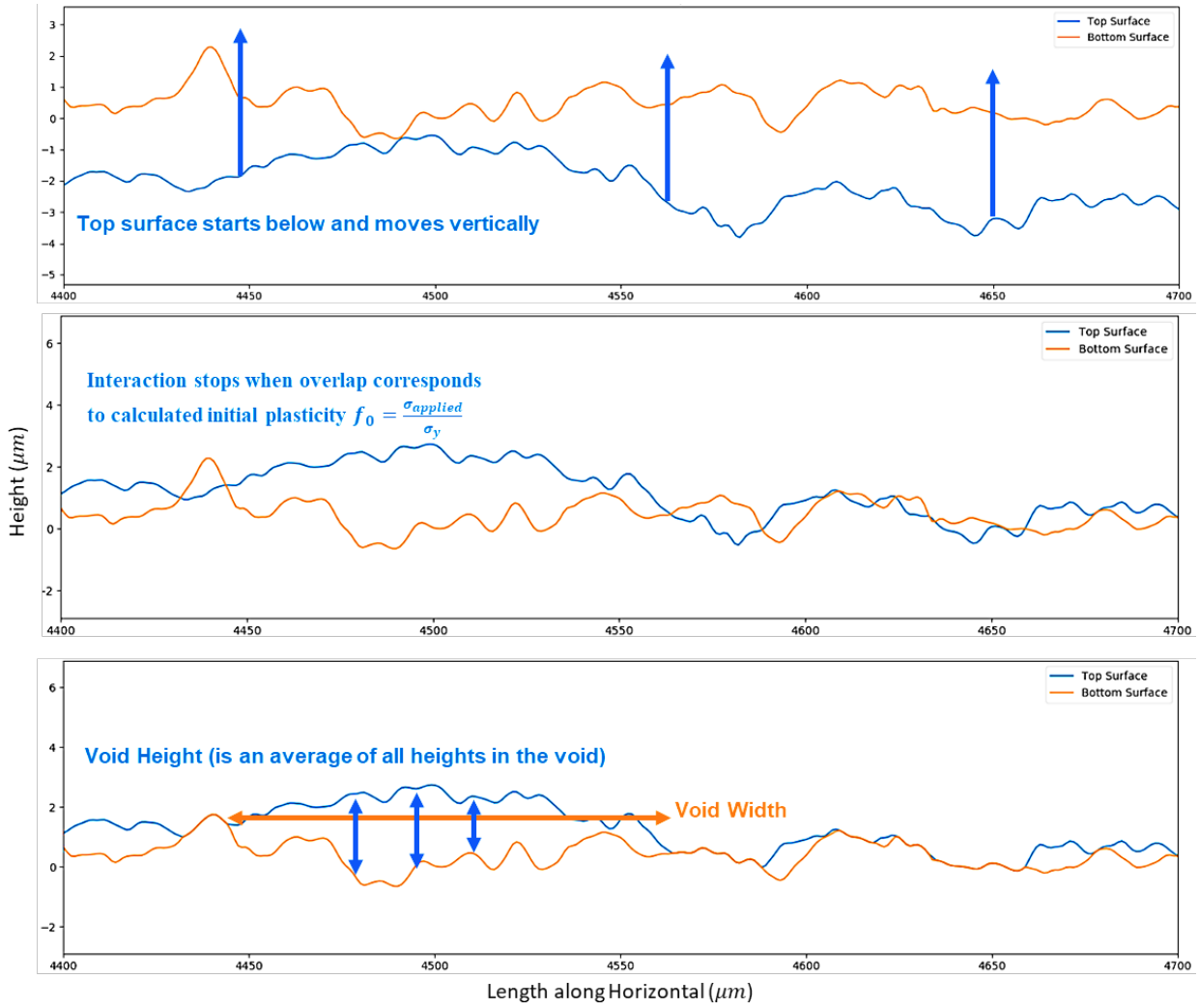

Figure 3: The surface profiles are overlapped to the point where they correspond. A calculated void is the average thickness over the specified width.

The surface profiles are in contact with each other until the overlap is at the same amount as specified in the Pilling model (the applied pressure over the yield strength of the material). For each of interactions between materials, one surface is translated relative to each. This is because there is no way of knowing exactly how the surface profiles will be mated in a production setting. This translation is repeated ten times in equal increments. Therefore, a total of 360 surface profile interactions per material combination are used to develop statistics on the void height and width. Figure 3 describes the algorithm procedure which entails flipping one of the profiles, translating it horizontally a given amount, overlapping it with the other profile until the contact stress would equal the yield strength, then determining the void height and width. The width of the void is the inside distance between each of the contact points. The height of the void is the average of the

Materials Research Proceedings **32** (2023) 338-354 https://doi.org/10.21741/9781644902615-39

overlap height between the contact points. These are used as the basis for Pilling's geometry in the stochastic model shown in Figure 4.

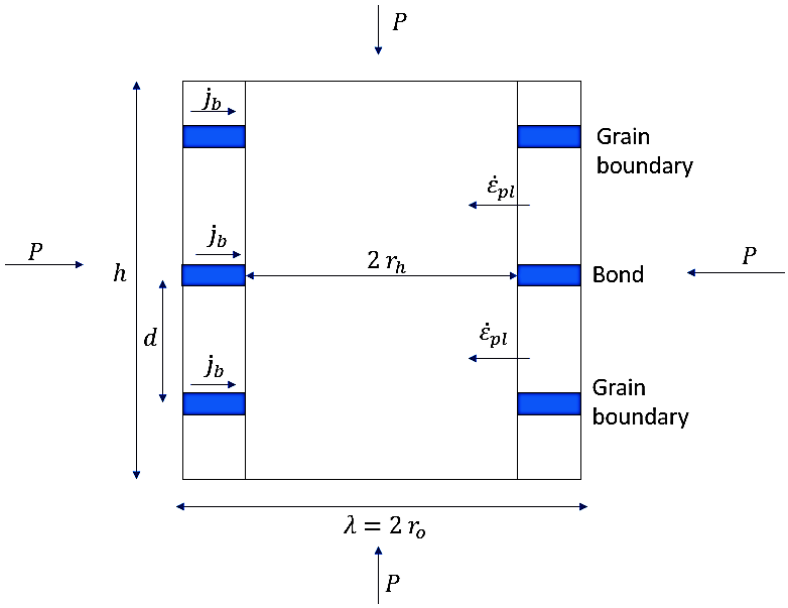

Figure 4: The Pilling void geometry is a revolved cylinder that has the axis of revolution along the bond plane normal vector.

The computed theoretical voids are tabulated and a distribution is fitted from the data. Many different statistical distributions were tried and the exponential distribution provided the best fit for both the height and the width of the voids. The void width had some significant outliers in the distribution where the surfaces randomly aligned to create an extremely large void. Void widths larger than the distribution fit maximum of 200 μm occurred around 7.5% of the time and were assumed to be negligible on the overall bonding performance. These large voids are most likely voids on the boundary of the surface profiles and would not occur in practice. An example of the distributions is presented in Figure 5.

a)

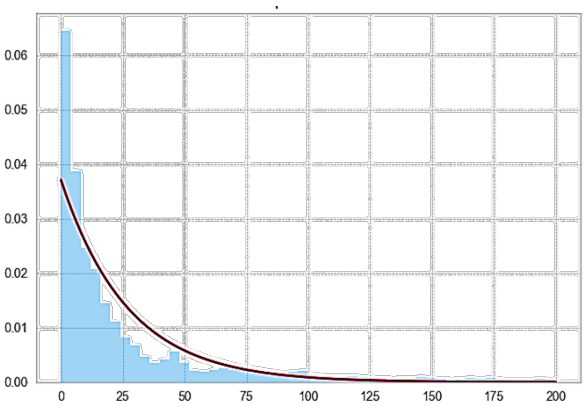

b)

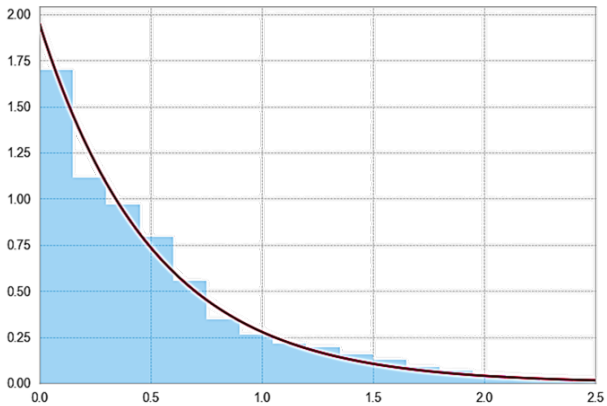

Figure 5: Example histogram of a) void width, and b) void height, with exponential distribution fits (Ti-54m/Ti-54m at low temperature and pressure).

Materials Research Proceedings **32** (2023) 338-354 https://doi.org/10.21741/9781644902615-39

The initial void geometry distributions are used as an input for a stochastic Pilling model. The primary equations were developed by Pilling and are for a specific void height and width. Using the probability distributions highlighted above, a random height and random width were selected. Then Pilling's equations were applied and the time required to completely bond was determined. The random selection of heights and widths and calculation of bonding was repeated 1000 times. Thus, a cumulative distribution was developed from the data to determine the percentage of randomly selected voids that would be closed after a given time for a set of processing conditions.

Pilling's equations are listed below in Eq. 1-7, and the explanation of terms along with the material properties are listed in Table 1. The initial bonding fraction, f, is determined by the applied stress divided by the high temperature yield strength of the material as shown in Eq. 1. The volume diffusion equation (Eq. 2), and the grain boundary diffusion equation (Eq. 3), were both derived from the stress dependent chemical potential due to the applied pressure. The plastic deformation from creep is modeled as deformation from an isostatic pressure with the creep equation (Eq. 4 and 5). The total change, bonded fraction per time, was integrated to determine the bonding time (Eq. 6). In a numerical implementation, the bonded fraction is incremented from the initial to complete closure while the height is kept uniform by applying the equations above. For each increment the change in time is computed. The bonding time for each random void is a summation of time increments. A flowchart of the simulation is provided in Figure 6.

$$f_0 = \frac{\sigma_{applied}}{\sigma_y}. \tag{1}$$

$$\left[\frac{df}{dt}\right]_{vol} = -\frac{4\Omega D_v}{kT}\left[\frac{f}{ln\left(\frac{1}{f}\right)-\frac{1-f}{2}}\right]\frac{1}{r_o^2}p. \tag{2}$$

$$\left[\frac{df}{dt}\right]_{gb} = -\frac{2\Omega D_{gb}\delta}{kT}\left[\frac{1}{ln\left(\frac{1}{f}\right)-\frac{1-f}{2}}\right]\frac{1}{r_o^2}p\left(\frac{1+\frac{h}{d}}{h}\right). \tag{3}$$

$$\dot{\varepsilon} = \frac{A\, exp^{(-Q_{sp}/RT)}\,\sigma^n}{T}. \tag{4}$$

$$\left[\frac{df}{dt}\right]_{plasticity} = \frac{-\dot{\varepsilon}}{\sigma_e}\left(3p\sqrt{f} - \frac{2\gamma\sqrt{f}}{r_0} + \frac{6\gamma}{r_0}\right). \tag{5}$$

$$t = \int_{f_0}^{f} \frac{-\sigma_e/\dot{\varepsilon}}{\left(-\frac{\dot{\varepsilon}}{\sigma_e}3p\sqrt{f} - \frac{2\gamma\sqrt{f}}{r_0} + \frac{6\gamma}{r_0}\right) + \frac{4\Omega D_v}{kT}\left[\frac{f}{\ln\left(\frac{1}{f}\right)-\frac{1-f}{2}}\right]\frac{1}{r_o^2}p + \frac{2\Omega D_{gb}\delta}{kT}\left[\frac{1}{\ln\left(\frac{1}{f}\right)-\frac{1-f}{2}}\right]\frac{1}{r_o^2}p\left(\frac{1+\frac{h}{d}}{h}\right)} df. \tag{6}$$

$$f(x;\mu,\lambda) = \left[\frac{\lambda}{2\pi x^3}\right] exp\frac{-\lambda(x-\mu)^2}{2\mu^2 x},\ (\text{for } x > 0, \mu > 0, \text{ and } \lambda > 0). \tag{7}$$

Table 1 – Material properties and variables for the Pilling equations (Pilling, 1988)

Properties	α	β
Atomic Volume, Ω (m^3)	1.76×10^{-29}	1.81×10^{-29}
Burgers vector, b (m)	2.9×10^{-10}	2.9×10^{-10}
Surface energy, γ (J m^2)	1.7	1.7
Grain boundary diffusivity, $D_{gb}\ \delta$	$3.6 \times 10^{-16} \times \exp(-97000/(R \times T))$	$5.4 \times 10^{-17} \times \exp(-153000/(R \times T))$
Grain boundary width, δ (m)	5.9×10^{-10}	5.72×10^{-10}
Volume boundary diffusivity, D_v	$8.6 \times 10^{-10} \times \exp(-150000/(R \times T))$	$1.9 \times 10^{-7} \times \exp(-153000/(R \times T))$
Shear modulus, G (MPa)	$4.3 \times 10^4 \times (1-((T-300)/T_m) \times 1.2)$	$2.05 \times 10^4 \times (1-((T-300)/T_m) \times 0.5)$
Creep constant, A	1.2×10^{-9}	1.2×10^{-9}
Strain rate creep constant, A_c	$A \times (D_{gb}\ \delta)_\alpha \times G_\alpha/(k \times T)$	$A \times (D_{gb}\ \delta)_\beta \times G_\beta/(k \times T)$
Gas constant, R (J/mol K)	8.314	
Botlzmann's constant, k (J/K)	1.38×10^{-23}	
Melting temperature, T_m (K)	1973	
Bonding temperature, T (K)	1046-1102	
Bonding pressure, P (MPa)	1-3	

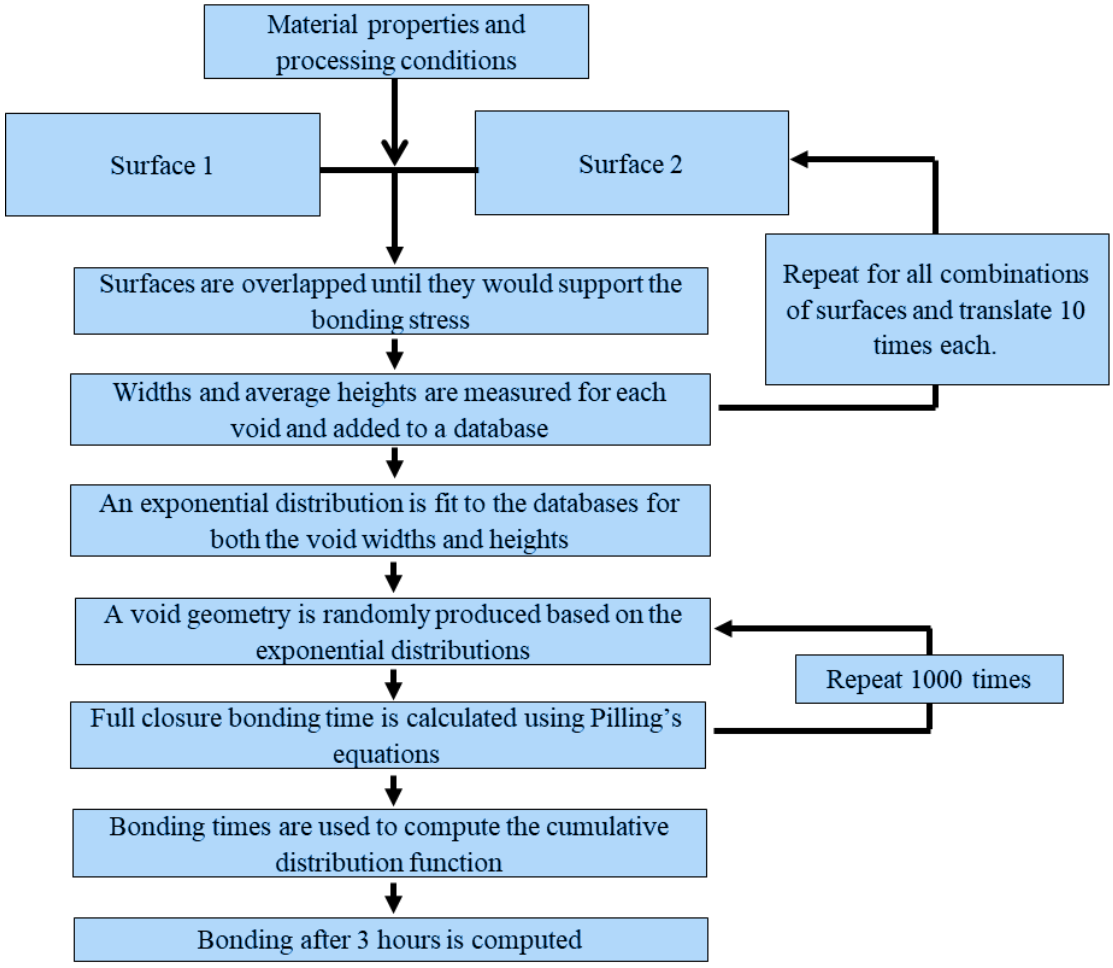

Figure 6: Program flowchart performed for each material combination and processing condition.

Materials Research Proceedings **32** (2023) 338-354 https://doi.org/10.21741/9781644902615-39

The simulation was compared with experimental data from TIMET, but the exact temperatures and pressure were not disclosed due to proprietary reasons. The pressures were labeled as low pressure (LP), intermediate pressure (IP), and high pressure (HP) while the temperatures were labeled as low temperature (LT), intermediate temperature (IT), and high temperature (HT). The grain sizes of the various materials are 2.4 μm for Ti-54M, 5.9 μm for Ti-64, and 4.1 μm for Ti-6242S [20]. The experimental results are summarized in Table 2 and are estimated from plots in the reference. The material properties for each of the calculations, shown in Table 1, is based on the rule of mixtures using the α/β ratio for each material. The α to β ratio depends heavily on the heat treatment of the alloys and is unknown for this data. The ratio is assumed to be 0.49 α for Ti-64 [21], 0.42 α for Ti-54m [22], and 0.33 α for Ti-6242 [23]. For every material/temperature/pressure combination the differences in α/β ratio generates a unique set of voids to be analyzed (54 unique sets).

Table 2 – Experimental results [20]

Materials	LT-LP	LT-IP	LT-HP	IT-LP	IT-IP	IT-HP	HT-LP	HT-IP	HT-HP
54m/54m	85%	95%	98%	100%	100%	100%	100%	100%	100%
64/64	51%	52%	53%	54%	81%	98%	91%	98%	99%
6242/6242	5%	8%	16%	37%	39%	49%	50%	59%	83%
54m/64	82%	95%	98%	100%	100%	100%	100%	100%	100%
54m/6242	44%	75%	81%	90%	95%	97%	98%	99%	100%
64/6242	17%	38%	47%	51%	60%	70%	70%	77%	97%

In addition to comparing work with published data, 9 conditions were simulated and experimentally verified in this study, which are shown in Table 3. Duplicate alloy combinations of Ti-6Al-4V fine grained (Ti-64FG to Ti-64FG), similar bonding of Ti-54M to Ti-54M), and dissimilar bonding with Ti-64FG to Ti-54M. Each condition was bonded at a moderate pressure for three hours. Each material combination was bonded at three temperatures, 0.530 T_m, 0.544 T_m, and 0.559 T_m, where T_m is the melting temperature. The details of the processing conditions are from [24].

Table 3 – Experimental data from specimens compared with predictions

Condition	Top Material	Bottom Material	Temperature	Experimental Bonded %	Calculated Bonded %
1	Ti-64 FG	Ti-64 FG	$0.530T_m$	64%	31%
2	Ti-64 FG	Ti-64 FG	$0.544T_m$	92%	83%
3	Ti-64 FG	Ti-64 FG	$0.559T_m$	100%	98%
4	Ti-54M	Ti-54M	$0.53T_m$	96%	24%
5	Ti-54M	Ti-54M	$0.544T_m$	100%	56%
6	Ti-54M	Ti-54M	$0.559T_m$	100%	100%
7	Ti-54M	Ti-64 FG	$0.530T_m$	95%	27%
8	Ti-54M	Ti-64 FG	$0.544T_m$	100%	73%
9	Ti-54M	Ti-64 FG	$0.559T_m$	100%	100%

Materials Research Proceedings **32** (2023) 338-354 https://doi.org/10.21741/9781644902615-39

Diffusion bonding specimens were created for each condition by taking two, clean and chemically milled, sheets of titanium and spot welding a sealing pattern around the perimeter. A gas tube was inserted and used to draw a vacuum between the sheets. Then the tube was welded shut leaving the vacuum between the sheets. The specimens were placed in a furnace at temperature and a superplastically expanding bladder was used to apply the bonding pressure. The specimens were cooled, sectioned and mounted, then ground using 200, 300, 400, 600, 800, and 1200 grit metallographic paper. Polishing was performed at 6 μm, 3 μm, and 1 μm diamond suspension, with a final polish of 0.05 μm alumina suspension with hydrogen peroxide. The specimens were etched for 10-15 seconds using Kroll's reagent, then imaged using an Olympus microscope at 500x. The bonding performance for each specimen was analyzed by looking at the percentage of bonded material along the bondline. The bonded fraction is the ratio of bonded material to total bond length along a simulated bondline, and the voids, and the bondline location, were determined by an image processing algorithm.

Results and Discussion

As discussed previously, none of the models provided a perfectly accurate fit to the experimental data and many of them cited specifically the lack of accurate surface geometry as a reason for this discrepancy. With the robust way of statistically incorporating the surface geometry presented in this paper, the surface effects should be well represented. However, as with the other bonding models, there were still some differences between the predicted bonding times and the experimental ones. The results of the simulation with respect to the experimental results is displayed in Figure 7. The high temperature – high pressure group was the most accurate of the processing conditions. However, some of the lower temperature and lower pressure groups had some significant inaccuracies. Figure 8 shows the average percentage discrepancy between experiments and calculations with respect to the temperature and pressure. The trend is fairly linear toward high pressure high temperature accuracy and low pressure low temperature inaccuracy.

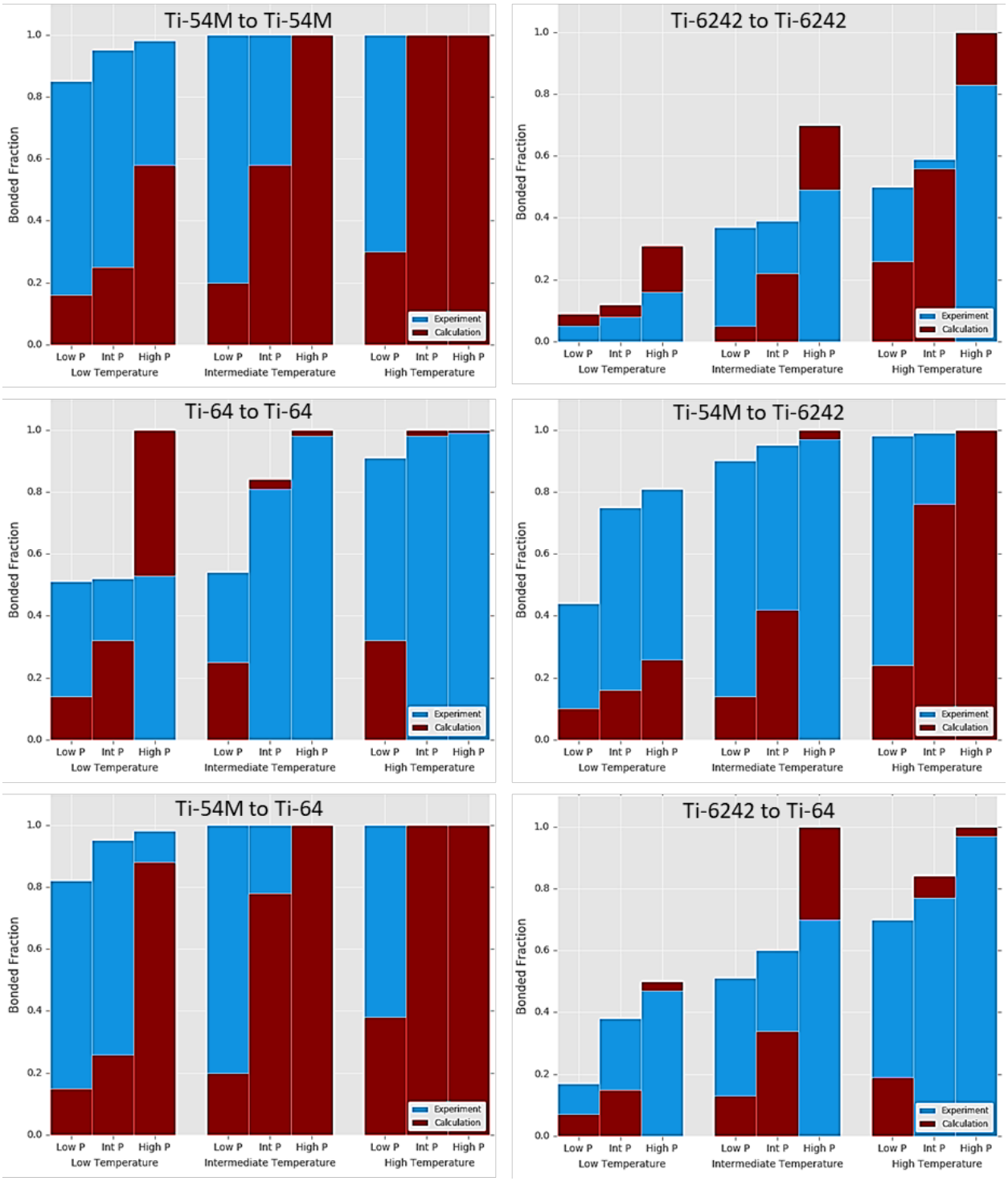

Figure 7: Program flowchart performed for each material combination and processing condition.

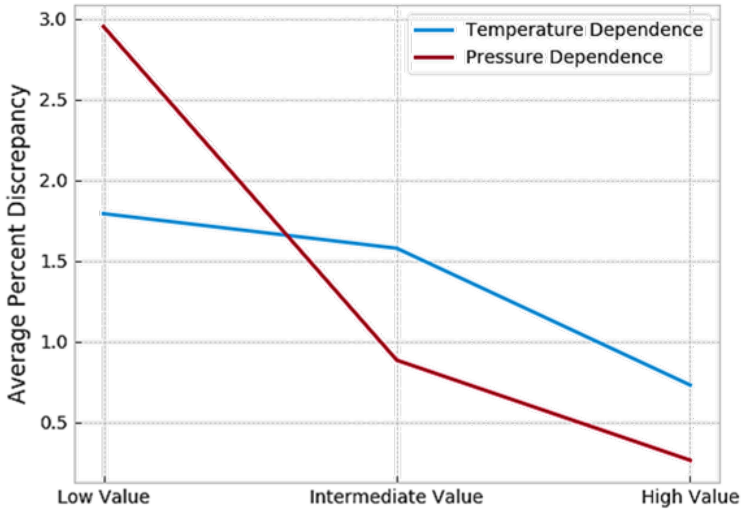

Figure 8: Average discrepancy between experimental data and calculated results by temperature and pressure. The high temperature and high pressure had the most accurate results.

While the theoretical aspects of a model determine its effectiveness, accurate material properties are also of paramount importance, and it is sometimes difficult to separate phenomenological issues with the theoretical model from discrepancies in the material properties. Specifically in this case, where the diffusion constants were based on the work of Ashby [24] which is a compilation of previous diffusion and deformation research from the 1960s-1980s, and it is meant for commercially pure titanium and not the alloys in this research. The material properties cited in previous titanium models separate the phases into α and β, and they have diffusion mobilities based on those two phases. Modern methods use the CALPHAD-type coupling of the thermodynamic and kinetic properties of a material to compute the diffusional mobilities making the diffusion of each alloying element a function of the Gibbs free energy and element concentrations [25,26]. Implementation of this would require more complex modeling of the different energies associated with the bonding process and is beyond the scope of this research. Therefore, some of the material properties used here and in other diffusion bonding research are most likely incorrect for these specific alloys.

To investigate how each material property is affecting the results of this simulation, a study was conducted. The effects of each parameter were calculated by using the base material properties in Table 1 along with the intermediate temperature and pressure and surface roughness constants for Ti-54M to Ti-54M at those processing conditions. By keeping everything else in the model constant and varying a single parameter, the relative change in complete bonding time is computed. For example, the temperature dependence in Figure 9 shows that if you reduce the temperature to 90% of the intermediate temperature, with all else being constant, the time required to obtain a fully bonded sample will increase by 7 times of what it would be at the intermediate temperature. The relative effects of each influential material property and processing condition is presented in a similar fashion.

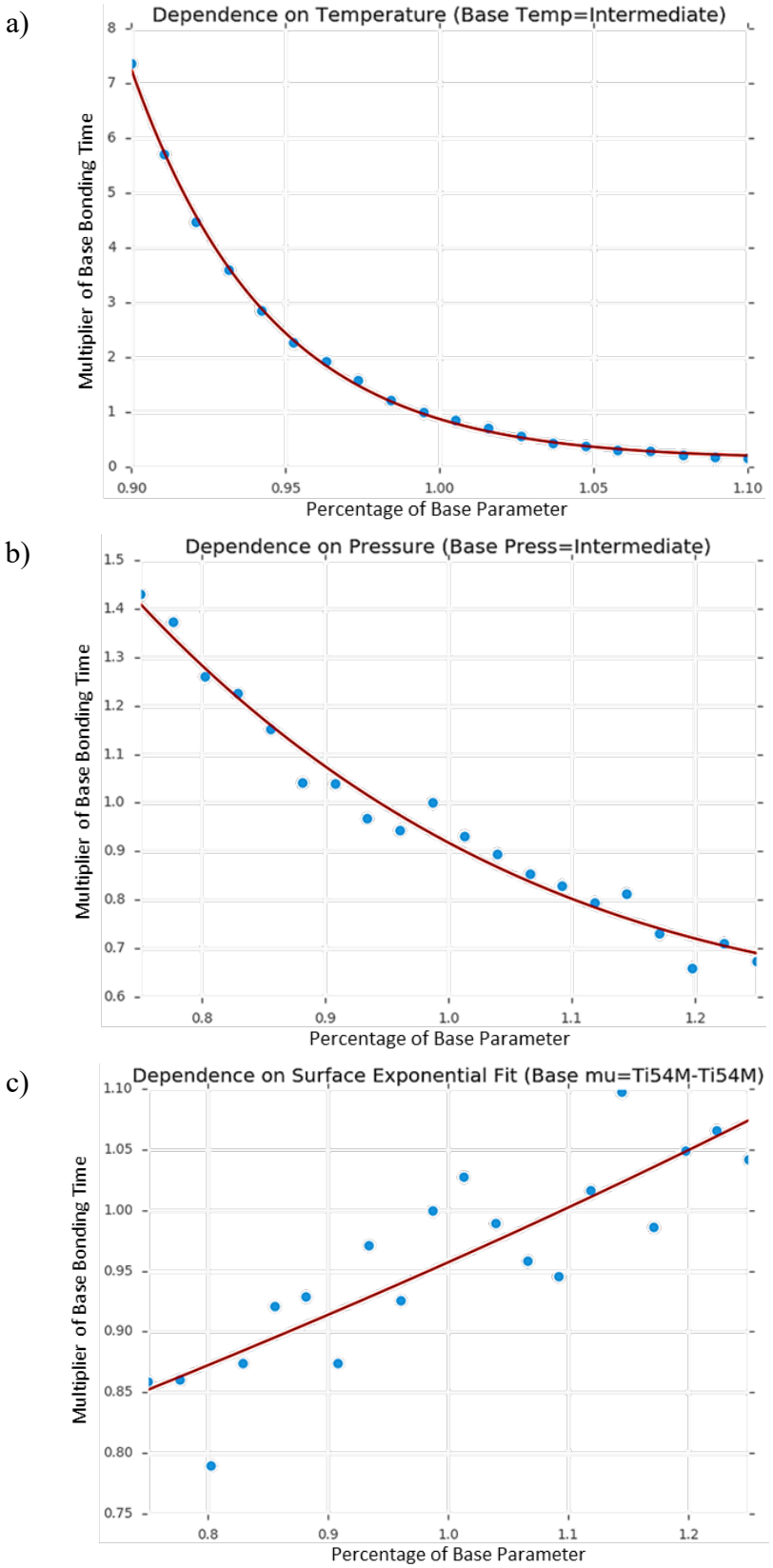

Figure 9: Dependencies on a) temperature, b) pressure, and c) surface parameter.

The primary processing conditions all have a strong effect on the bonding performance in the model and are in line with expectations. Most significant, is the temperature which softens the

Materials Research Proceedings **32** (2023) 338-354 https://doi.org/10.21741/9781644902615-39

material for better closure during initial contact, increases the different diffusion constants, and increases the creep strain as the temperature increases providing a lower bonding time. A higher pressure provides more stress for power law creep and diffusion which reduces bonding time. As the surface parameter reduces, representing a distribution of smaller voids, the bonding time decreases while a larger surface parameter takes longer to close due to the larger voids. The effect of the surface is less extensive than the effects of temperature and pressure which is to be expected.

The material constants for the β phase are less conducive to bonding than the α phase. The amount of α and β will change depending on processing and heat treatment. Since the exact heat treatments were unknown for these materials, and the $\beta\%$ was unknown, the assumed α/β ratio could be a source of inaccuracy. For those papers that have investigated the rates of the different bonding mechanisms, creep has been the dominant bonding mechanism [2,10,13,15]. Pilling's model was no exception, and the bonding time was significantly affected by the creep material constants as shown in Figure 10. There is some debate as to whether the mechanism of plastic collapse is due to power-law creep (as in Derby and Hill's pressure sintering models), or if it is due to superplastic collapse (Hamilton and Pilling's models). While the equations are similar, the creep exponent is three times larger for power-law creep versus superplastic deformation. There are many additional constants that were checked but have no strong influence on the bonding time. Most notably is the grain size, which had no discernable influence, but is additionally incorporated into this version of Pilling's model and Hill's model.

A variation of parameters could be performed to determine exactly which combination of modified material properties allows this model to fit the experimental data accurately. However, this is unphysical and does not demonstrate the effectiveness of the model which is the point of this research. Because creep is the dominant closure mechanism, the creep exponent is the most influential material property, but the exact value of the exponent is unknown for these alloys, and there is some debate on the exponent value. Anyway, it is sufficient to modify this parameter alone in order to demonstrate how sensitive the results are to this material property. By lowering the creep exponent slightly more toward diffusive creep, Coble creep, and Nabarro-Herring creep, the accuracy of the model significantly increases especially in the lower temperature range. The changes in accuracy of the model simplify by a 0.025, 0.05, and 0.075 reduction in creep exponent which corresponds to an decrease in the average discrepancy between experiments and simulation from 28.32% to 23.0%, 19.5%, and 19.2% respectively. This demonstrates how sensitive these material properties can be and how measuring them on the specific alloys modeled would be necessary for an accurate diffusion bonding model.

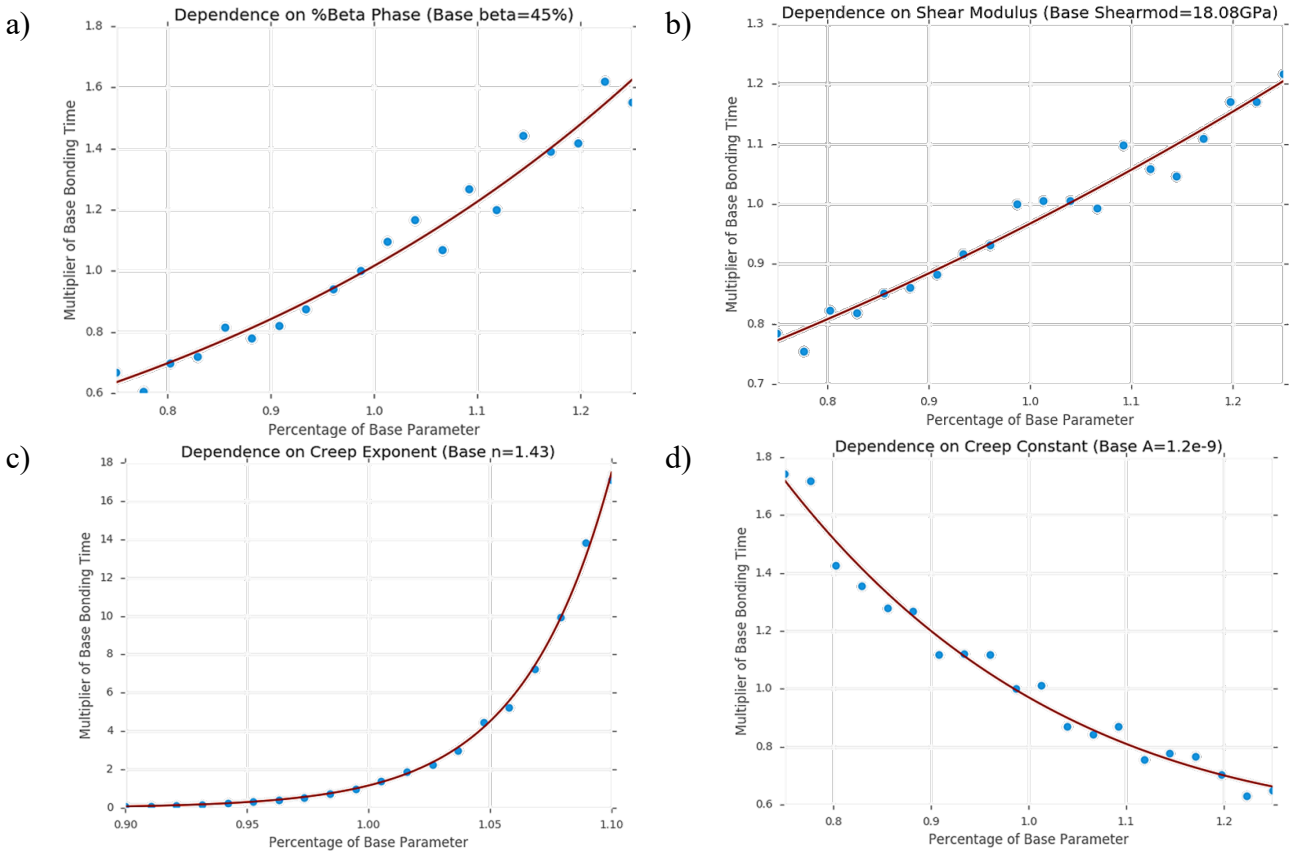

Figure 10: Dependence on a) alpha/beta ratio, b) shear modulus, c) creep exponent, and d) creep constant.

Summary

The stochastic Pilling model was computed with significantly more robust initial conditions computed through interactions of surface profiles. A database of potential voids was produced by overlapping several different surface roughness profiles in multiple ways to the overlap specified by the initial conditions of the diffusion bonding model. Pilling's model was then used to determine the statistical bonding percentage for the bonding time. While the model predicted the high temperature high pressure group very well, it was less accurate for other cases. An investigation into the effects of different material constants was performed, and comments were made on specific material properties that could cause issues. Further research could include simulations of different theoretical models in a similar fashion, implementation into three dimensions, and creation of an energy-based simulation with more modern material properties.

Acknowledgements

The authors sincerely thank The Boeing Company for funding the SPF/DB research at University of Washington. In addition, MR wants to acknowledge the Boeing-Pennell professorship funding and EB would like to acknowledge the Boeing Learning Together Program for educational funding.

References

[1] D. G. Sanders and M. Ramulu, "Examination of superplastic forming combined with diffusion bonding for titanium: Perspective from experience," J. Mater. Eng. Perform., vol. 13, no. 6, pp. 744-752, Dec. 2004. https://doi.org/10.1361/10599490421574

[2] A. Hill and E. Wallach, "Modelling solid-state diffusion bonding," Acta Metall., vol. 37, no. 9, pp. 2425-2437, 1989. https://doi.org/10.1016/0001-6160(89)90040-0

[3] M. F. Islam, J. Pilling, and N. Ridley, "Effect of surface finish and sheet thickness on isostatic diffusion bonding of superplastic Ti-6Al-4V," Mater. Sci. Technol., vol. 13, no. 12, pp. 1045-1050, Dec. 1997. https://doi.org/10.1179/mst.1997.13.12.1045

[4] H. Somekawa and K. Higashi, "The optimal surface roughness condition on diffusion bonding," Mater. Trans., vol. 44, no. 8, pp. 1640-1643, 2003. https://doi.org/10.2320/matertrans.44.1640

[5] A. Wang, O. Ohashi, and K. Ueno, "Effect of surface asperity on diffusion bonding," Mater. Trans., vol. 47, no. 1, pp. 179-184, 2006. https://doi.org/10.2320/matertrans.47.179

[6] C. H. Hamilton, "Pressure requirements for diffusion bonding titanium," Titan. Sci. Technol., pp. 625-648, 1973. https://doi.org/10.1007/978-1-4757-1346-6_46

[7] B. Derby and E. R. Wallach, "Diffusion bonding: development of theoretical model," Met. Sci., vol. 18, no. 9, pp. 427-431, 1984. https://doi.org/10.1179/030634584790419809

[8] B. Derby and E. R. Wallach, "Diffusion bonds in copper," J. Mater. Sci., vol. 19, no. 10, pp. 3140-3148, 1984. https://doi.org/10.1007/BF00549797

[9] B. Derby and E. R. Wallach, "Theoretical model for diffusion bonding," Met. Sci., vol. 16, no. 1, pp. 49-56, 1982. https://doi.org/10.1179/030634582790427028

[10] Z. X. Guo and N. Ridley, "Modelling of diffusion bonding of metals," Mater. Sci. Technol., vol. 3, no. 11, pp. 945-953, 1987. https://doi.org/10.1179/mst.1987.3.11.945

[11] Y. Takahashi and K. Inoue, "Recent void shrinkage models and their applicability to diffusion bonding," Mater. Sci. Technol., vol. 8, no. 11, pp. 953-964, 1992. https://doi.org/10.1179/mst.1992.8.11.953

[12] J. Pilling, D. W. Livesey, J. B. Hawkyard, and N. Ridley, "Solid state bonding in superplastic Ti-6Al-4V," Met. Sci., vol. 18, no. 3, pp. 117-122, 1984. https://doi.org/10.1179/msc.1984.18.3.117

[13] J. Pilling, "The kinetics of isostatic diffusion bonding in superplastic materials," Mater. Sci. Eng., vol. 100, pp. 137-144, 1988. https://doi.org/10.1016/0025-5416(88)90249-2

[14] M. T. Salehi, J. Pilling, N. Ridley, and D. L. Hamilton, "Isostatic diffusion bonding of superplastic Ti-6Al-4V," Mater. Sci. Eng. A, vol. 150, no. 1, pp. 1-6, 1992. https://doi.org/10.1016/0921-5093(90)90002-K

[15] N. Orhan, M. Aksoy, and M. Eroglu, "A new model for diffusion bonding and its application to duplex alloys," Mater. Sci. Eng. A, vol. 271, no. 1, pp. 458-468, 1999. https://doi.org/10.1016/S0921-5093(99)00315-9

[16] R. Ma, M. Li, H. Li, and W. Yu, "Modeling of void closure in diffusion bonding process based on dynamic conditions," Sci. China Technol. Sci., vol. 55, no. 9, pp. 2420-2431, Sep. 2012. https://doi.org/10.1007/s11431-012-4927-1

[17] S.-X. Li, S.-T. Tu, and F.-Z. Xuan, "A probabilistic model for prediction of bonding time in diffusion bonding," Mater. Sci. Eng. A, vol. 407, no. 1-2, pp. 250-255, Oct. 2005. https://doi.org/10.1016/j.msea.2005.07.003

[18] N. Kulkarni, M. Ramulu, and D. G. Sanders, "Modeling of Diffusion Bonding Time in Dissimilar Titanium Alloys: Preliminary Results," J. Manuf. Sci. Eng., vol. 138, no. 12, p. 121010, 2016. https://doi.org/10.1115/1.4034133

[19] F. A. Calvo, J. G. De Salazar, A. Urena, J. G. Carrion, and F. Perosanz, "Diffusion bonding of Ti-6Al-4V alloy at low temperature: metallurgical aspects," J. Mater. Sci., vol. 27, no. 2, pp. 391-398, 1992. https://doi.org/10.1007/BF00543928

[20] P. P. Gudipati and Y. Kosaka, "Diffusion Bonding of Similar and Dissimilar Titanium Alloys," presented at the Proceedings of the 13th World Conference on Titanium, 2016, pp. 1631-1636. https://doi.org/10.1002/9781119296126.ch273

[21] S. Jadhav, A. Powar, S. Patil, A. Supare, B. Farane, and R. Singh, "Effect of volume fraction of alpha and transformed beta on the high cycle fatigue properties of bimodal Ti6Al4V alloy," IOP Conf. Ser. Mater. Sci. Eng., vol. 201, p. 012035, May 2017. https://doi.org/10.1088/1757-899X/201/1/012035

[22] Y. Kosaka and P. GUDIPATI, "Method for the manufacture of alpha-beta ti-al-v-mo-fe alloy sheets," EP2721187 A1, 23-Apr-2014.

[23] M. E. Kassner, Y. Kosaka, and J. S. Hall, "Low-cycle dwell-time fatigue in Ti-6242," Metall. Mater. Trans. A, vol. 30, no. 9, pp. 2383-2389, 1999. https://doi.org/10.1007/s11661-999-0246-y

[24] P. M. Sargent and M. F. Ashby, "Deformation maps for titanium and zirconium," Scr. Metall., vol. 16, no. 12, pp. 1415-1422, 1982. https://doi.org/10.1016/0036-9748(82)90439-2

[25] L. Huang, Y. Cui, H. Chang, H. Zhong, J. Li, and L. Zhou, "Assessment of Atomic Mobilities for bcc Phase of Ti-Al-V System," J. Phase Equilibria Diffus., vol. 31, no. 2, pp. 135-143, Apr. 2010. https://doi.org/10.1007/s11669-009-9641-8

[26] Y. Liu, Y. Ge, D. Yu, T. Pan, and L. Zhang, "Assessment of the diffusional mobilities in bcc Ti-V alloys," J. Alloys Compd., vol. 470, no. 1, pp. 176-182, Feb. 2009. https://doi.org/10.1016/j.jallcom.2008.02.111